ACES

DOI: 10.1002/asia.201500303

CHEMISTRY
AN ASIAN JOURNAL
Full Paper

Fluorescence | *Very Important Paper* |

VIP Influences of Conjugation Extent on the Aggregation-Induced Emission Quantum Efficiency in Silole Derivatives: A Computational Study

Yujun Xie,[a, b] Tian Zhang,[c] Zhen Li,[b] Qian Peng,*[a] Yuanping Yi,[a] and Zhigang Shuai*[c]

Abstract: The photophysical properties of a series of silole derivatives, with hydrogen (TPS), bromine (BrTPS), and conjugated phenyl (HPS), triphenylsilyethynyl (BTPES), and dimethylfluorene (BFTPS) substituents at 2,5-positions in both gas and aggregate phases have been investigated computationally by employing the correlation function rate formalism coupled with a hybrid quantum/molecular mechanics (QM/MM) approach. It is found that the solid-state fluorescence quantum efficiency first increases sharply with the degree of π-conjugation of the 2,5-substituents, then levels off, and finally starts to decrease slightly. This is because the side-group conjugation tends to enhance the radiative decay rate in both gas and solid phases. However, a further increase in conjugation leads to saturation in the radiative decay rate but increases the non-raditiave decay rate due to the decreased energy gap.

Introduction

Recently, siloles (silacyclopentadienes) have received much attention as promising molecules for organic electroluminescent devices[1] owing to their unusual electronic structure,[2] high electron mobilities,[3] and especially, their exotic aggregation-induced emission (AIE) behavior.[4] The peculiar electronic structure of siloles is mainly attributed to the lowest unoccupied molecule orbital (LUMO) involving σ*–π* conjugation between the σ* orbital over the exocyclic Si–C bonds and the π* orbital of the cis-butadiene fragment.[2] There have been efforts to explore the effect of substituents at 1,1-, 2,5-, and 3,4-positions of the central silole ring on the electronic structures and photophysical properties.[2b,5] As conjugation was broken by the silicon atom, substituents on the silicon atom at 1,1-positions are largely inductive in nature and have a minor impact on the optical emission or electron transport.[2b,5d,6] The 3,4-substituents are largely twisted with respect to the silacycle plane with torsion angles of about 50° either from X-ray crystal structures or computational optimized structures, which leads to disruption of conjugation with the central silacycle. Through studying the fluorenyl-substituted siloles, it is found that for aryl substituents at 3,4-positions, the inductive effects dominate over orbital delocalization.[2b,6b] Aryl substituents at 2,5-positions have a more pronounced influence on the electronic and optical properties through a strong conjugation effect. As observed experimentally, the siloles without aryl substituents at 2,5-positions exhibit a weak emission in both solution and aggregate states.[5b] The aryl-substituted siloles at 2,5-position display highly intense solid-state emission.[7] However, further elongation of conjugation tends to decrease the fluorescent quantum efficiency in the solid state.[5a,g] It is primarily the motivation of this work to investigate the conjugated and non-conjugated substitution effect on the solid-state emission for the AIE systems, typified by siloles. The AIE mechanism in siloles has been investigated theoretically and experimentally through temperature effects, steric effects, aggregation effects, and so on.[8,9] It has been found that the restriction of intramolecular rotation and the blocking of the non-radiative decay process are the main causes for the enhanced fluorescence in the solid state compared with those in dilute solutions. In this work, we systematically study the influence of different substituents at 2,5-positions on the photophysical properties for a series of silole derivatives at the first-principles level.

Here, we chose five 1,1,3,4-tetraphenyl siloles derivatives where the 2,5-substituents have different electron-withdrawing abilities and different conjugation degrees, that is, hydrogen (TPS),[5b] bromine (BrTPS),[6a] phenyl (HPS),[5d] triphenylsilylethynyl (BTPES),[6a] and 9,9-dimethylfluoren-2-yl (BFTPS)[6b] to calcu-

[a] *Y. Xie, Dr. Q. Peng, Dr. Y. Yi*
Key Laboratory of Organic Solids
Beijing National Laboratory for Molecular Science (BNLMS)
Institute of Chemistry
Chinese Academy of Sciences
Beijing 100190 (China)
E-mail: qpeng@iccas.ac.cn

[b] *Y. Xie, Prof. Z. Li*
Department of Chemistry
Wuhan University
Wuhan 430072 (China)

[c] *T. Zhang, Prof. Z. Shuai*
Key Laboratory of Organic OptoElectronics and Molecular Engineering
Department of Chemistry
Tsinghua University
Beijing 100084 (China)
E-mail: zgshuai@tsinghua.edu.cn

Supporting information for this article is available on the WWW under http://dx.doi.org/10.1002/asia.201500303.

late the radiative and non-radiative decay rate constants, both in gas and solid phases, in order to gain insights into the influences of 2,5-substituents on the optical emission efficiency for the molecular design of novel materials.

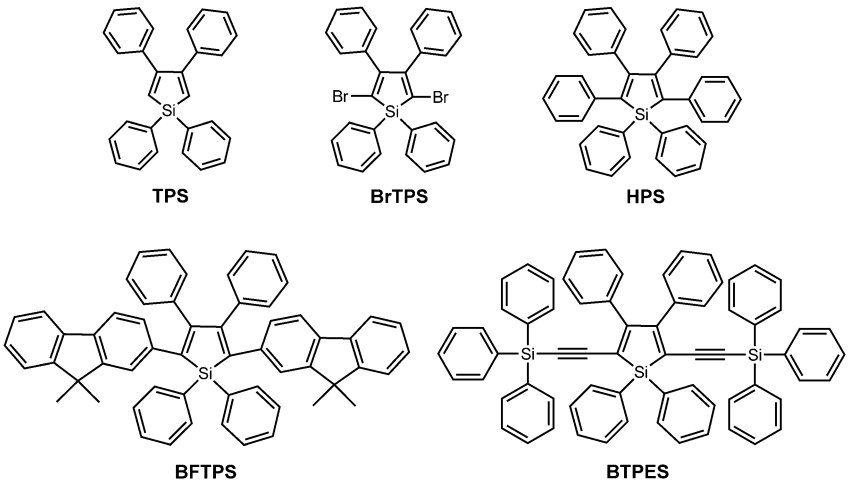

Results and Discussion

Geometrical and electronic structures

In Table 1 and Table S1 in the Supporting Information, we present the optimized major geometrical structure parameters of the ground and excited states for the five compounds both in gas and solid states, as well as the corresponding X-ray crystal structure data for comparison. The calculated geometrical structures at S_0 minimum in the solid phase are in good aggreement with the crystal structures for all the compounds, with the largest deviation being less than 4° for angles and 0.03 Å for bond lengths. These confirm the reliability of our combined QM/MM approach with B3LYP/SV(P) and general Amber force field (GAFF) (see the Experimental Section). It should be noted that the optimized clockwise and anticlockwise forms have equal energies and electric dipole moments for the isolated compounds. Compared with the molecules in cluster, the isolated molecules are more flexible. Upon photoexcitation, the geometrical modifications between S_0 and S_1 states are much larger for isolated molecules than in clusters. For TPS and BrTPS, the torsional angle at the 3-position exhibits great changes of 13.67° and 18.24° in the gas phase, far larger than those in the solid state of 3.65° and 2.15°. Once the atoms at 2,5-positions are substituted by rotational conjugated groups, the biggest changes occur at the torsional angles of 2,5-substituents rather than those of 3,4-substituents. In the gas phase, the former are 12.52° and 15.66° for HPS, and 20.55° and 20.60° for BFTPS, while the latter are less than ~7.0° for all the siloles. In the solid state, the torsional angles of the 2,3,4,5-substituents for all the siloles vary slightly with changes less than 8.0°. At the same time, the molecular bond lengths of double bonds are elongated and those of single bonds are shortened for cis-butadiene units when excited from S_0 to S_1 states. In addition, for HPS, BTPES, and BFTPS, the torsional angles of 2,5-substituents at S_0/S_1-geometries are always much smaller than those of 3,4-substituents in both gas and solid phases, indicating that the 2,5-substituents are conjugated better with the central silole ring. The extent of conjugation increases in the order of TPS < BrTPS < HPS < BTPES < BFTPS.

As shown previously,[2,8,25] in both solid and gas phases, the HOMO is of π character, whereas the LUMO contains the conjugated σ*–π* feature, namely, the exocyclic C–Si bonds display σ* character and the butadiene moiety shows π* character. The electronic density contours of HOMO and LUMO in the solid and gas phases are shown in Figure 1 and Figure S2, respectively. As can be seen in Figure 1, the HOMO of TPS mainly localizes on the central silacycle and the 3,4-phenyl rings, indicating congugation between the 3,4-phenyl rings and the central silacycle. This is also manifested by the small

Table 1. Selected geometrical parameters of dihedral angles (in degree) for the siloles at S_0 and S_1 states in the gas and solid phases.

	TPS			BrTPS			HPS			BTPES			BFTPS		
	S_0	S_1	$\lvert\Delta(S_0\text{-}S_1)\rvert$	S_0	S_1	$\lvert\Delta(S_0\text{-}S_1)\rvert$	S_0	S_1	$\lvert\Delta(S_0\text{-}S_1)\rvert$	S_0	S_1	$\lvert\Delta(S_0\text{-}S_1)\rvert$	S_0	S_1	$\lvert\Delta(S_0\text{-}S_1)\rvert$
Gas phase															
2-							−37.0	−24.5	12.5				−42.7	−22.2	20.6
5-							−40.2	−24.6	15.7				−42.8	−22.2	20.6
3-	46.8	33.1	13.7	−59.2	−41.0	18.2	−57.1	−51.4	5.6	53.3	49.6	3.7	−58.1	−55.3	2.8
4-	46.9	42.0	4.9	−59.1	−60.5	1.4	−57.0	−51.5	5.6	52.0	45.5	6.5	−58.0	−55.3	2.8
Solid phase															
2-							40.5	33.6	7.3				31.4	27.0	4.4
5-							4.4	1.9	1.9				31.4	27.0	4.4
3-	40.2	36.6	3.7	−53.0	−50.9	2.2	62.8	55.5	6.8	−59.1	−54.7	4.4	58.1	54.4	3.7
4-	49.2	45.4	3.8	−53.0	−50.9	2.2	83.9	85.8	2.5	−45.5	−43.2	2.3	58.1	54.4	3.7

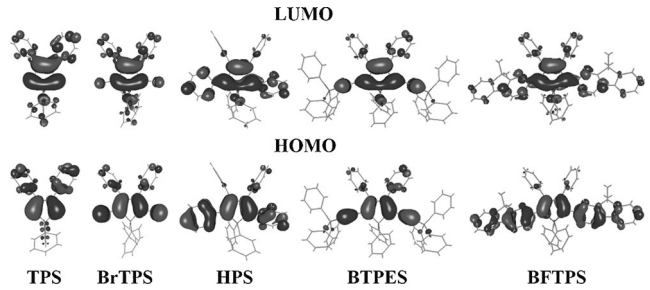

Figure 1. Electron density contours of HOMO and LUMO for the siloles in the solid phase at the B3LYP/SV(P) level (contour level = 0.03)

torsional angle for 3,4-phenyl rings. When bromine atoms were introduced to the 2,5-positions of TPS replacing hydrogen, the contribution to the HOMO from bromine is quite large owing to the effect of the lone pair electron while the contribution from 3,4-phenyls is immediately reduced. Furthermore, when the 2,5-substitutents become the conjugated groups in HPS, BTPES, and BFTPS, the HOMOs almost completely delocalize over the 2,5-substituents and the central silacycle, with almost no contribution from the 3,4-phenyls. This suggests that the conjugated groups at 2,5-position strengthen the molecular conjugation effect. As a result, as seen in Figure 2, the energies of HOMOs increase in the order of TPS < HPS < BFTPS caused by the pure conjugation effect, and BrTPS < BTPES because of the balance between the conjugation effect and the electron-withdrawing effect of −Br and −$Si(Ph)_3$. Different from HOMO, LUMOs not only delocalized over the same groups in HOMO but also spread over to the Si atom and C atom of 1,1-phenyl because of the σ^*–π^* conjugate effect (Figure 1). As expected, contrary to HOMO, the LUMO levels decrease in the order of TPS > HPS > BFTPS and BrTPS > BTPES with the extended conjugation of 2,5-substituents for the siloles (Figure 2). Altogether, the 2,5-substitution tends to significantly decrease the gap in the order of TPS > BrTPS > HPS > BTPES > BFTPS in accord with the extension of the conjugation. The charge density features of HOMO and LUMO are very similar for the siloles in solid and gas phases (Figure S2).

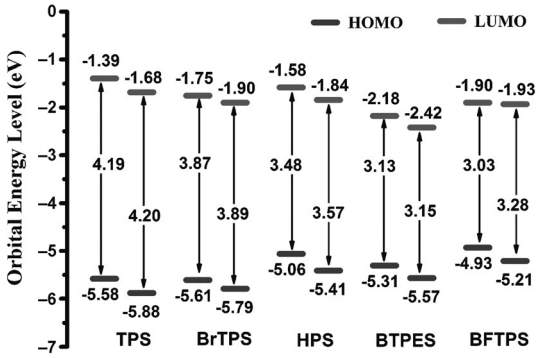

Figure 2. Frontier orbital energy level of the five compounds in gas (right) and solid (left) phases.

Due to the polarization effect, the energy level in the solid state is shifted with respect to the gas phase, and the energy gaps show a slight red-shift (Figure 2).

Based on the optimized S_0/S_1-geometries, the vertical excitation energies (VEE) were calculated, corresponding to the absorption/emission maximum peak positions based on the Franck–Condon principle. The calculated optical spectral parameters in cluster are compared with the corresponding available experimental data measured in thin film or crystal for the siloles in Table 2. The deviations between the calculated and experimental values lie between 0.18 and 0.41 eV, which is reasonable.[11] The calculated Stokes shifts reproduce even better the experimental values with the largest deviation being less than 10 nm for the siloles except for BTPES. These data indicate that (i) the adopted funtional B3LYP and basis set SV(P) are appropriate to decrible the electronic structure of the siloles; (ii) TDDFT is applicable for the siloles because their S_1 state mainly stems from the transition from the HOMO to the LUMO with a component of > 97% (Table S2 in the Supporting Information). It can also be seen from Table 2 that both the absorption and emission spectra are red-shifted, in line with the increase of conjugation degree of TPS < BrTPS < HPS < BTPES < BFTPS induced by 2,5-substituents.

Table 2. The calculated and the experimental optical spectrum parameters for the five siloles in the solid phase.

	Absorption		Emission		Stokes shift	
	Calc. [eV nm^{-1}]	Exp. [eV nm^{-1}]	Calc. [eV nm^{-1}]	Exp. [eV nm^{-1}]	Calc.[nm]	Exp.[nm]
TPS	4.00/310	4.31/288[a]	2.80/443	3.17/392[a]	133	104[a]
BrTPS	3.35/370	–	2.50/497	–	127	–
HPS	3.07/404	3.36/369[b]	2.35/528	2.53/490[b]	124	121[b]
BTPES	2.77/447	3.06/405[c]	2.21/561	2.55/487[c]	114	82[c]
BFTPS	2.60/478	3.01/412[d]	2.03/611	2.35/529[d]	133	117[d]

[a] See ref. [5b]. [b] See ref. [5i]. [c] See ref. [6a]. [d] See ref. [6b].

Radiative decay rate constants

The radiative decay rate constants, calculated as shown in Table 3, increase with the conjugation degree of 2,5-substituents going up from TPS to BFTPS either in gas or solid states except that the ones of HPS and BTPES in the solid state are very close. From the spontaneous emission relationship, the radiative rate constant is proportional to the electric transition dipole moment and the excitation energy between the ground and excited states. We firstly looked at the electric transition dipole moment (TDM) as a function of 2,5-substituents. Taking the center of silacycle as the coordinate origin and the silacycle plane as *y-z* plane, we evaluated the electric TDM from the S_1 to S_0 at S_1-geometry in both gas and solid states. The total TDM vectors are plotted in Figure 3 for the gas phase, while those for the solid phase are shown in Figure S3 in the Supporting Information. It is found that (i) TPS has a quite small TDM value due to the poor conjugation between the 3,4-phe-

Table 3. The calculated k_r and k_{IC} values (s^{-1}), and the fluorescence quantum efficiencies of the five siloles in gas phase and solid phases, as well as the available experimental data (given in parenthesis).

	Gas phase			Solid phase		
	k_r	k_{IC}	η_F	k_r	k_{IC}	η_F
TPS	9.30×10^5	1.62×10^{10}	0.01% (0.02%)[a]	1.15×10^6	3.32×10^6	25.8% (16.8%)[a]
BrTPS	5.55×10^6	5.72×10^9	0.09% (–)	8.12×10^6	1.50×10^6	82.3% (–)
HPS	4.98×10^7	2.53×10^{10}	0.20% (0.22%)[b]	7.43×10^7	1.57×10^6	97.9% (78%)[b]
BTPES	6.76×10^7	2.66×10^{10}	0.25% (2.3%)[c]	6.57×10^7	1.93×10^6	97.1% (18.1%)[c]
BFTPS	1.22×10^8	1.66×10^9	6.86% (2.6%)[d]	1.14×10^8	1.07×10^7	91.4% (88%)[d]

Note: $\eta_F = k_r/(k_r + k_{IC} + k_{ISC})$ for BrTPS with $k_{ISC} = 2.65\times10^8\ s^{-1}$ in gas phase and $k_{ISC} = 2.30\times10^5\ s^{-1}$ in the solid phase, and $\eta_F = k_r/(k_r + k_{IC})$ for other four siloles. [a] See ref. [5b]. [b] See ref. [5i]. [c] See ref. [6a]. [d] See ref. [5f].

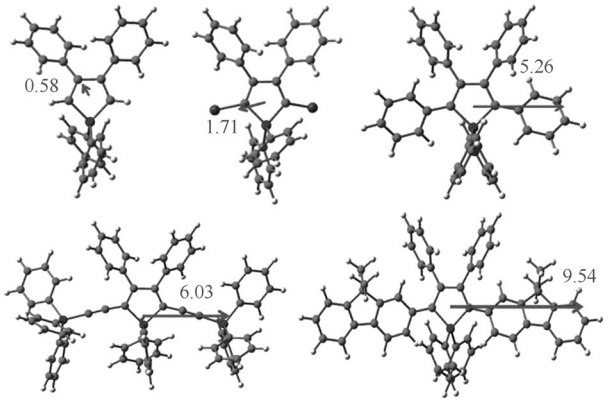

Figure 3. The transition dipole moment vectors (unit: Debye) from S_1 to S_0 at the S_1-geometry for the isolated siloles.

nyls and the central silacycle; (ii) when the bromine atoms are introduced at 2,5-positions, the TDM vector changes from *x* and *y* to the *z* direction (orientation of 2,5-substituent) and the amount is more than doubled. Moreover, with increasing degree of 2,5-substituent conjugation, the TDM value increases drastically. These data suggest that the conjugated 2,5-substituents induce a large electric TDM due to the electron delocalization. Such an increase surpasses the decrease in energy gap and leads to an ascending order for the radative decay rates: $k_r(TPS) < k_r(BrTPS) < k_r(HPS)$, $k_r(BTPES) < k_r(BFTPS)$. This trend of the radiative decay rate is the same in both gas and solid phases.

Internal conversion rate constants

It is most appropriate to elaborate the excited-state reorganization energy, or relaxation energy here. It can be obtained by using the four-point method according to the adiabatic potential energy surfaces of the ground and excited states:

$$\lambda_g = E_g(S_1 - \text{geometry}) - E_g(S_0 - \text{geometry}) \quad (1)$$

$$\lambda_e = E_e(S_0 - \text{geometry}) - E_e(S_1 - \text{geometry}) \quad (2)$$

where $E_{g(e)}(S_{1(0)}\text{-geometry})$ is the energy of the ground (excited) at the S_1 (S_0) equilibrium geometry. Under the harmonlic oscillator approximation, λ_g and λ_e can be also expressed as a summation over all the normal mode:

$$\lambda_g = \sum_{k=1}^{3n-6} \lambda_{g,k} = \sum_{k=1}^{3n-6} 1/2\omega_{g,k}^2 \Delta D_k^2 \quad (3)$$

$$\lambda_g = \sum_{k=1}^{3n-6} \lambda_{e,k} = \sum_{k=1}^{3n-6} 1/2\omega_{e,k}^2 \Delta D_k^2 \quad (4)$$

Here $\omega_{g(e),k}$ represents the frequency of the k^{th} normal mode at the ground (excited) state, and ΔD_k is the displacement along the k^{th} normal mode coordinate between the equilibrium positions of two electronic states. The results of the TDDFT calculation are given in Table 4. The agreement between the two approaches rationalizes the applicability of the harmonic model.

Table 4. Reorganization energies λ_{gs} and λ_{es} obtained by normal modes and adiabatic poential energy surface (in parenthesis).

		TPS	BrTPS	HPS	BTPES	BFTPS
gas phase	λ_{gs} [meV]	639 (637)	665 (643)	405 (397)	339 (314)	374 (350)
	λ_{es} [meV]	481 (448)	496 (473)	486 (471)	328 (310)	447 (425)
solid phase	λ_{gs} [meV]	513 (441)	470 (435)	377 (363)	309 (265)	304 (291)
	λ_{es} [meV]	419 (424)	420 (419)	376 (361)	283 (298)	303 (278)

Both our previous work[13] and Table 3 reveal that the k_{IC} in the gas phase is typically several orders of magnitude larger than that in the solid phase because the rotational motions of low-frequency normal modes are largely depressed in the solid phase for many AIE molecules including siloles. The prefactor in the IC rate formula in Equation (9), the nonadiabatic electronic coupling term, hardly varies when going from an isolated molecule to cluster (Figure S4 in the Supporting Information). As far as the excited-state reorganization energy λ is concerned (Figure S3 in the Supporting Information), we can identify two vibration reigons, one with low frequency ($< 200\ cm^{-1}$) and the other with high frequency (1200–1600 cm^{-1}) for both gas and solid phases (Table S3 in the Supporting Information). This feature is similar for all the substituted siloles studied here. The former is assigned to the rotational motion of peripheral aromatic groups and the latter to the stretching vibrations of carbon–carbon bonds of silacycle, as shown in Figure S6 in the Supporting Information. The total reorganization energy in the gas phase is much larger than that in cluster, which is largely caused by the restriction on the low-

Table 5. The reorganization energy projected into the geometry relaxation of internal coordinate for the siloles in gas and solid phases (in meV).

	TPS		BrTPS		HPS		BTPES		BFTPS	
	gas	solid	gas	solid	gas	solid	gas	solid	gas	solid
λ_{BL} [a]	282	293	293	297	270	285	229	228	240	217
λ_{DA} [b]	132	63	135	51	183	52	69	28	192	54
$\lambda_{DA\ 2,5-sub.}$ [b]					139	24			166	26
$\lambda_{DA\ 3,4-sub.}$ [b]	67	34	61	30	31	21	20	20	5	15

[a] BL = bond length. [b] DA = dihedral angle.

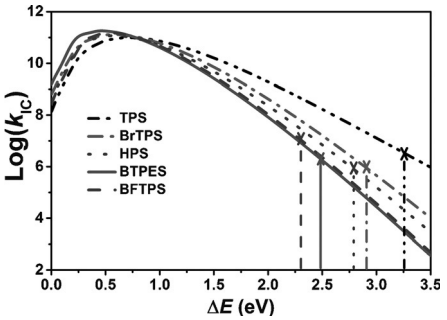

Figure 4. The calculated log(k_{IC}) spectra versus energy gap (eV) of five siloles in the solid phase. The real values of log(k_{IC})s are localized at $\Delta E = \Delta E_{ad}$, marked by an X.

frequency motions going from the gas to solid phase. By projecting the reorganization energy into the geometry relaxation in the internal coordinates (Table 5), it is found that the reduction mainly stems from the rotational angles of the aromatic ring, for example, 3,4-substituents of TPS and BrTPS and 2,5-substituents of HPS and BFTPS. Such features are in good correspondence with the geometrical modifications from S_1 to S_0 states.

In order to better understand the factors governing the k_{IC} and to estabilish the property–structure relationship, we present an approximate form of k_{IC} by assuming (i) the promoting mode is not displaced, (ii) all the modes are not distorted, (iii) the Duschinsky rotation effect is ignored, and (iv) the short-time approximation is adopted:

$$\ln(k_{IC}) = -\frac{1}{4\sum_k' \lambda_{k\neq l}\bar{E}_k}\left(\Delta E_{ad} - \hbar\omega_l - \sum\nolimits_{k\neq l}' \lambda_k\right)^2 \quad (5)$$

$$+\ln\left(\frac{1}{\hbar^2}\left(\frac{\omega_l}{2\hbar}|R_l|^2\right)\sqrt{\frac{\pi}{\sum_{k\neq l}' \lambda_k \bar{E}_k}}\right)$$

where $\bar{E}_k = (\bar{n}_k + 1/2)h\omega_k$ and $\bar{n}_k = [\exp(h\omega_k/kT) - 1]^{-1}$ are the average vibration energy and phonon occupation number, respectively. From Equation (5) it is easily seen that ln(k_{IC}) versus ΔE_{ad} is a downward parabola with the axis of symmetry of $\Delta E_{ad} = \hbar\omega_l + \sum_{k\neq l}' \lambda_k$ and latus rectum of $4\sum_k' \lambda_k \bar{E}_k$. Thus, the adiabatic excitation energy ΔE_{ad} and the reorganization energy λ are the two important factors to control the k_{IC}. We plotted log(k_{IC}) as a function of the energy gap ΔE for the five siloles in cluster in Figure 4. When ΔE is equal to the adiabatic excitation energy ΔE_{ad} the corresponding value is the k_{IC}. It should be noted that for the internal conversion rate from S_1 to S_0, the ΔE_{ad} is always far larger than the sum of the total reorganization energy and the energy of the promoting normal mode, that is $\Delta E_{ad} \gg \hbar\omega_l + \sum_{k\neq l}' \lambda_k$. In such a case, the k_{IC} decreases sharply with ΔE. Moreover, when ΔE is large enough, ln(k_{IC}) decreases approximately linearly with ΔE, namely, the energy gap law. The adiabatic excitation energies of the sioles are going down from TPS to BFTPS, which would bring about the decrease of the non-radiative rate constant according to Equation (5). Further, the parabola becomes narrower with a decrease of the reorganization energy. With the extension of the molecular conjugation, the total reorganization energy ($\lambda_{gs} + \lambda_{es}$) decreases and then tends to saturate from TPS to BFTPS, with values of 932 cm^{-1} for TPS, 890 cm^{-1} for BrTPS, 753 cm^{-1} for HPS, 592 cm^{-1} for BTPES, and 607 cm^{-1} for BFTPS (Table 4). As shown in Figure 4, the k_{IC} spectra are correspondingly first narrowed down rapidly and then tend toward overlap. Altogether, the competition between the two factors causes the IC rate constant first to decrease, then to level off, and finally to increase from TPS to BFTPS as seen in Table 3 and Figure 4. At the same time, this suggests that when the reorganization energy is left largely unchanged, the energy gap law mainly governs the IC rate constants.

Fluorescence quantum efficiency

The de-excitation pathways of the molecular excited-state consist of not only the intramolecular emission of fluorescence, non-radiative internal conversion (IC) from S_1 to S_0 and intersystem crossing (ISC) from S_1 and $T_{n\ (n \geq 1)}$, and conformational change, but also the intermolecular electron transfer, proton transfer, energy transfer, excimer or exciplex formation, and so on. The molecular conformational change, intermolecular electron/proton transfers, and excimer/exciplex formations always lead to new fluorescent species, whose emission can be distinguished from the "primary" fluorescence arising from the excited molecule. For the studied siloles, the difference between fluorescence spectra in dilute solution and thin films are minor, suggesting that there is no new species generated by the interaction between molecules. Hence, the fluorescence quantum efficiency (FQE) from the first excited singlet state to the ground state can be calculated as $\eta_F = k_r/(k_r + k_{IC} + k_{ISC})$. The intersystem crossing rate constant highly depends on the spin-orbit coupling (SOC) and the energy gap between S_1 and T_n states. Generally, pure organic molecules have an extremely small spin-orbit coupling. Adachi et al. have noted that the ISC process would be fast (around 10^6–10^7 s^{-1}) when the energy gap between S_1 and T_1 levels is as small as 100 meV in pure organic molecules.[12] In Table S5, we present the energy differences and spin-orbit coupling constants between S_1 and T_n which lie below S_1 at S_1-geometries for the siloles in the gas phase. We found that the energy difference between S_1 and T_1 are more than 1.4 eV for the siloles, and their SOC constants are very small with values less than 0.32 cm^{-1} expect for BrTPS of 3.04 cm^{-1} owing to the heavy atom effect of the bromine

atom. The SOC constant of BrTPS in the solid state is 2.96 cm^{-1}, slightly smaller than that in the gas phase. Therefore, in calculating the FQE, we do not take the ISC rate constant into account except for BrTPS, whose k_{ISC} is calculated to be 2.65×10^{8} s^{-1} in the gas phase and 2.30×10^{5} s^{-1} in the solid state. That is, $\eta_F = k_r/(k_r + k_{IC} + k_{ISC})$ was used for the FQE of BrTPS while $\eta_F = k_r/(k_r + k_{IC})$ was adopted for the other four siloles. The calculated results are plotted in Figure 5 and the detailed data are seen in Table 3 in comparison with available experimental values. The calculated FQEs are in good agreement with the experimental values for the siloles both in gas and solid states except for BTPES in the solid state. Such discrepancy could be ascribed to the amorphous nature of thin film which is modeled as a perfect crystal. From Figure 5, we clearly observed the exotic phenomena of aggregation-induced emission for the siloles with the FQEs in the solid state far larger than those in the gas phase. We also found that for the siloles in the solid state, the FQE firstly increases from TPS to HPS, and then decreases from HPS to BFTPS. From TPS to HPS, the radiative decay rates rise very rapidly, while the non-raditive decay rates vary slightly. This is because the introduction of the conjugated 2,5-substituents sharply enhances the TDM (and oscillator strength). In contrast, from HPS to BFTPS, the non-radiative decay rates increase by one order of magnitude owing to the significant reduction in the adiabatic excitation energy, while the change of the radiative decay rates is small. Therefore, with the degree of conjugation of 2,5-substituents increasing, the FQE exhibits a level-off and then a small-decrease behavior.

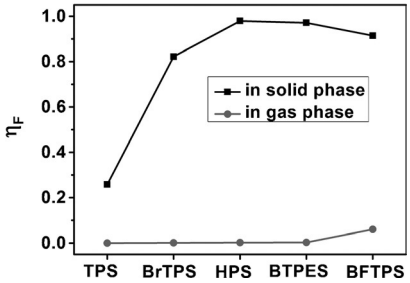

Figure 5. The calculated fluorescence quantum efficiency for the silole derivatives with increasing degree of conjugation in gas and solid states.

Conclusion

We comparatively investigated the electronic structures, the excited-state decay, and the fluorescence quantum efficiency for a series of silole derivatives with increasing degree of conjugation, from hydrogen, electron-withdrawing bromine, conjugated phenyl, triphenylsilyethynyl to dimethylfluorene substituents at 2,5-positions, using vibration correlation function theory combined with QM/MM calculation. We found that the conjugated substituents at 2,5-positions play an essential role in tuning the fluorescence quantum efficiency in the solid state. The electronic conjugation at 2,5-substituents tends to get involved in the electronic excitation, significantly increasing the transition dipole moment from 0.58 Debye for TPS to 9.54 Debye for BFTPS. Correspondingly, the radiative decay rates are increased by more than two orders of magnitude from 9.3×10^{5} s^{-1} for TPS to 1.22×10^{8} s^{-1} for BFTPS. It was understood before that the aggregation-induced emission in siloles stems from the suppression of the non-radiative decay channels with the restriction of the rotational/vibrational motions of peripheral aromatic groups with respect to the central silacycle (especially, groups at 2,5-positions). With increasing molecular conjugation in the order of TPS < BrTPS < HPS < BTPES < BFTPS, the reorganization energy, favoring the non-radiative decay rate, first decreases and then saturates to some extent; while the energy gap, disfavoring the non-radiative decay, decreases monotonically. Moreover, the energy gap law ultimately dominates the IC rate constants when the reorganization energy tends to become a constant. The competition between the two factors causes the IC rate constant first to decrease, then to level off, and finally to increase from TPS to BFTPS. Altogether, the calculated solid-state fluorescence quantum efficiency first increases sharply with the degree of conjugation, then levels off, and finally starts to decrease slightly. This behavior is in agreement with experimental results for other silole derivatives,[5a,g] implying the possibility to control the aggregate fluorescence quantum effiency through molecular design.

Finally, it should be noted that the excited state dynamics consists of the most challenging issue in theoretical and computational chemistry.[14] The presented approach we developed earlier[16] with subsequent improvements[23] has been based on the assumptions of perturbation theory and harmonic oscillator model, among other approximations. It has indeed demonstrated robustness in describing the aggregation effects on the light emission.[13] Further developments considering intermolecular charge delocalization and excitonic effect are in progress. Mixed quantum-classical excited state dynamics simulation[15] has also been shown to achieve some qualitative success, if not quantitative. It is still a long way to go toward quantitative prediction of solid-state luminescence quantum efficency from first-principles.

Experimental Section

Theoretical methodology and computational approach

Electronic structure

The molecular geometry optimizations and frequency calculations were performed for the ground state (S_0) and the first excited triplet state (T_1) at the B3LYP/SV(P) level, and for the first excited singlet state (S_1) at the TD/B3LYP/SV(P) level. These were carried out with the Turbomole 6.5 program.[16] We mimicked the solid state effect through a combined quantum mechanics and molecular mechanics (QM/MM) by cutting a big cluster from the experimental crystal stucture, where the central molecule is the QM part and its surroundings are MM regions (see Figure 6 and Figure S1 in the Supporting Informa-

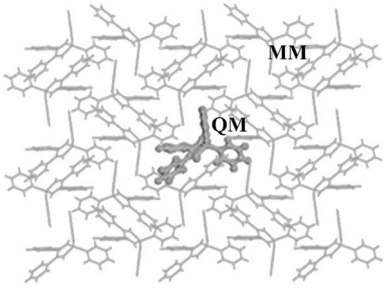

Figure 6. Setup of QM/MM computational model taking TPS as an example: one central QM molecule and the surrounding 73 MM molecules.

tion). The interaction between the two parts is through electrostatic Hamiltonian.[17] The central QM region provides important information for the electronic excited state while the surrounding MM region contains the essential corrections from the environment, neglecting the excitonic effect as well as the intermolecular charge transfer. This approximation is appropriate for most of silole derivatives, since their intermolecular distances are very large and always exceed 7.0 Å and the luminescent spectral peaks in the solid phase coincide well with those in solution phase, that is, the intermolecular distances of the studied silole derivatives lie in the range of 7.2–12.5 Å. The QM molecule is described at the same level with as that for the compounds in the gas phase described above. The MM molecules are modeled through the general Amber force field (GAFF).[18] The QM/MM was interfaced by using the ChemShell 3.5 package.[19] Turbomole 6.5 and DLPOLY[20] programs were used to calculate the energies and energy gradients of the QM/MM, respectively. The electrostatic embedding scheme with QM polarization was adopted. Note that during the QM/MM geometry optimizations, the QM molecule was active while the MM region was kept frozen. The vibrational frequencies were obtained by using a numerical two-point displacement method and the electric polarization of the environment was included. No symmetric constraint was adopted for the geometric optimizations.

Excited-state non-radiative decay rate constant

Under the framework of the first-order perturbation theory, the general non-radiative decay rate constant can be written as[21]

$$k_{NR} = \frac{2\pi}{\hbar}\sum_{u,v} P_{iv}\left|\hat{H}'_{fu,iv}\right|^2 \delta(E_{iv} - E_{fu}) \tag{6}$$

Here, P_{iv} is the Boltzmann distribution function; E_{iv} (E_{fu}) represents the electronic and vibrational energy of the initial (final) state; the perturbation Hamiltonian $\hat{H}'$ includes the spin-orbit coupling $\hat{H}^{SO}$ and Born-Oppenheimer coupling $\hat{H}^{BO}$ beyond the adiabatic approximation:

$$\hat{H}'\Psi_{iv} = \hat{H}^{BO}\Phi_i(\mathbf{r};\mathbf{Q})\Theta_v(\mathbf{Q}) + \hat{H}^{SO}\Phi_i(\mathbf{r};\mathbf{Q})\Theta_v(\mathbf{Q}) \tag{7}$$

where Φ and Θ are the wavefunctions for electrons and nuclei, respectively. In most cases, the term $\partial^2\Phi_i/\partial_{fl}^2$ is very small and often overlooked. Thus, the first term reads:

$$\hat{H}^{BO}\Phi_i\Theta_{iv} = \hbar^2\sum_l \frac{\partial\Phi_i}{\partial Q_l}\frac{\partial\Theta_{iv}}{\partial Q_l} = \sum_l \hat{P}_l\Phi_i\hat{P}_l\Theta_{iv} \tag{8}$$

where l is the index of the normal mode and $\hat{P}_{fl}$ is the normal momentum operator of the l-th normal mode.

By applying the Franck–Condon principle, the non-radiative internal conversion (IC) rate constant for the transition between the two electronic states within the same spin manifold can be expressed as:[22]

$$k_{IC} = \frac{2\pi}{\hbar}\sum_{kl} R_{kl}Z_i^{-1}\sum_{v,u} e^{-\beta E_{iv}}P_{kl}\delta(E_{iv} - E_{fu}) \tag{9}$$

where $R_{kl} = \langle\Phi_f|\hat{P}_{fk}|\Phi_i\rangle\langle\Phi_i|\hat{P}_{fl}|\Phi_f\rangle$ is the non-adiabatic electronic coupling, and the nuclear momentum integral is: $P_{kl} = \langle\Theta_{fu}|\hat{P}_{fk}|\Theta_{iv}\rangle\langle\Theta_{iv}|\hat{P}_{fl}|\Theta_{fu}\rangle$.

Equation (9) can be reduced to a compact analytic form with the thermal vibration correlation function (TVCF) by using the Fourier transform of the delta function,

$$k_{IC} = \sum_{kl}\frac{1}{\hbar^2}R_{kl}\int_{-\infty}^{\infty} dt\left[e^{i\omega_{if}t}Z_i^{-1}\rho_{IC}(t,T)\right] \tag{10}$$

where $\rho_{IC}(t,T)$ is the TVCF of $Tr\left(\hat{P}_{fk}e^{-i\tau_f\hat{H}_f}\hat{P}_{fl}e^{-i\tau_i\hat{H}_i}\right)$.

Similarly, the non-radiative intersystem crossing (ISC) rate constant for the transition between two electronic states with different spin state reads,[23]

$$k_{IC} = \frac{1}{\hbar^2}\langle\Phi_f|\hat{H}^{SO}|\Phi_i\rangle\int_{-\infty}^{\infty} dt\left[e^{i\omega_{if}t}Z_i^{-1}\rho_{ISC}(t,T)\right] \tag{11}$$

where $\rho_{ISC}(t,T) = Tr\left[e^{-i\tau_f\hat{H}_f}e^{-i\tau_i\hat{H}_i}\right]$ is the same as the Franck–Condon factor.

The TVCFs have been solved analytically by using multidimensional Gaussian integrations in our previous works.[23,24]

For calculating the non-radiative decay rate constant, the difference between the potential energy surfaces of the two relevant electronic states were considered with $\underline{Q}_i = \underline{S}\underline{Q}_f + \underline{D}$. Here S is the Duschinsky rotation matrix and D is the displacement vector, where both can be calculated by following Reimers' algorithm.[24,25] The first-order non-adiabatic coupling terms were computed by using the exact analytical derivative couplings between time-dependent Kohn–Sham (TDKS) determinants in a finite atom-centered basis set, which has been implemented in EGRAD excited-state gradient module of TURBOMOLE program developed by Furche et al.[26] The spin-orbit coupling matrix elements were calculated at the TDDFT level[27] with the first-order DKH-like spin-orbit operator derived from the exact two-component Hamiltonian[28] as implemented in BDF program package.[29] Finally, the internal conversion and

intersystem crossing rate constants were evaluated by using the thermal vibration correlation function method briefly described above with our home-built MOMAP program.[30]

Excited-state radiative decay rate constant

The radiative decay rate constant was calculated by using the simple spontaneous emission relationship of $k_r = 1/1.499\ f\ \Delta E^2$ for a two-level system. It has been shown to give good results for organic molecules.[8] Here, f is the dimensionless oscillator strength and ΔE is the energy difference in the unit of cm^{-1} between S_1 and S_0 states at the optimized S_1-geometry. These parameters were calculated at the level of TDDFT.

Acknowledgements

This work is supported by the Ministry of Science and Technology of China through 973 program (Grant Nos.2013CB834703 and 2015CB655002) and the National Natural Science Foundation of China (Grant Nos. 21290191, 21303213, and 91333202) as well as the Strategic Priority Research Program of the Chinese Academy of Sciences (Grant XDB12020200).

Keywords: aggregation-induced emission · excited state radiative and non-radiative decay rate constants · fluorescence quantum efficiency · QM/MM calculation · photophysics · siloles

[1] a) K. Geramita, J. McBee, Y. Shen, N. Radu, T. D. Tilley, *Chem. Mater.* **2006**, *18*, 3261 – 3269; b) Z. Zhao, S. M. Chen, J. W. Y. Lam, C. K. W. Jim, C. Y. K. Chan, Z. M. Wang, P. Lu, C. M. Deng, H. S. Kwok, Y. G. Ma, B. Z. Tang, *J. Phys. Chem. C* **2010**, *114*, 7963 – 7972; c) H. J. Son, W. S. Han, J. Y. Chun, C. J. Lee, J. I. Han, J. Ko, S. O. Kang, *Organometallics* **2007**, *26*, 519 – 526.

[2] a) S. Yamaguchi, K. Tamao, *J. Chem. Soc. Dalton Trans.* **1998**, 3693 – 3702; b) X. Zhan, S. Barlow, S. R. Marder, *Chem. Commun.* **2009**, 1948 – 1955.

[3] a) K. Tamao, M. Uchida, T. Izumizawa, K. Furukawa, S. Yamaguchi, *J. Am. Chem. Soc.* **1996**, *118*, 11974 – 11975; b) M. Uchida, T. Izumizawa, T. Nakano, S. Yamaguchi, K. Tamao, K. Furukawa, *Chem. Mater.* **2001**, *13*, 2680 – 2683.

[4] a) J. Luo, Z. Xie, J. W. Y. Lam, L. Cheng, H. Chen, C. Qiu, H. S. Kwok, X. Zhan, Y. Liu, D. Zhu, B. Z. Tang, *Chem. Commun.* **2001**, 1740 – 1741; b) A. Qin, J. W. Y. Lam, B. Z. Tang, *Prog. Polym. Sci.* **2012**, *37*, 182 – 209.

[5] a) B. Chen, H. Nie, P. Lu, J. Zhou, A. Qin, H. Qiu, Z. Zhao, B. Z. Tang, *Chem. Commun.* **2014**, *50*, 4500 – 4503; b) E. Zhao, J. W. Y. Lam, Y. Hong, J. Liu, Q. Peng, J. Hao, H. H. Y. Sung, I. D. Williams, B. Z. Tang, *J. Mater. Chem. C* **2013**, *1*, 5661; c) T. Jiang, Y. Jiang, W. Qin, S. Chen, Y. Lu, J. W. Y. Lam, B. He, P. Lu, H. H. Y. Sung, I. D. Williams, H. S. Kwok, Z. Zhao, H. Qiu, B. Z. Tang, *J. Mater. Chem.* **2012**, *22*, 20266; d) J. W. Chen, C. C. W. Lam, J. W. Y. Lam, Y. P. Dong, S. M. F. Lo, I. D. Williams, D. B. Zhu, B. Z. Tang, *Chem. Mater.* **2003**, *15*, 1535 – 1546; e) S. Yamaguchi, T. Endo, M. Uchida, T. Izumizawa, K. Furukawa, K. Tamao, *Chem. Eur. J.* **2000**, *6*, 1683 – 1692; f) B. Chen, Y. Jiang, L. Chen, H. Nie, B. He, P. Lu, H. H. Sung, I. D. Williams, H. S. Kwok, A. Qin, Z. Zhao, B. Z. Tang, *Chem. Eur. J.* **2014**, *20*, 1931 – 1939; g) B. Chen, Y. Jiang, B. He, J. Zhou, H. H. Sung, I. D. Williams, P. Lu, H. S. Kwok, H. Qiu, Z. Zhao, B. Z. Tang, *Chem. Asian J.* **2014**, *9*, 2937 – 2945; h) J. Mei, J. Wang, J. Z. Sun, H. Zhao, W. Yuan, C. Deng, S. Chen, H. H. Y. Sung, P. Lu, A. Qin, H. S. Kwok, Y. Ma, I. D. Williams, B. Z. Tang, *Chem. Sci.* **2012**, *3*, 549 – 558.

[6] a) Z. Zhao, D. Liu, F. Mahtab, L. Xin, Z. Shen, Y. Yu, C. Y. Chan, P. Lu, J. W. Lam, H. H. Sung, I. D. Williams, B. Yang, Y. Ma, B. Z. Tang, *Chem. Eur. J.* **2011**, *17*, 5998 – 6008; b) X. Zhan, A. Haldi, C. Risko, C. K. Chan, W. Zhao, T. V. Timofeeva, A. Korlyukov, M. Y. Antipin, S. Montgomery, E. Thompson, Z. An, B. Domercq, S. Barlow, A. Kahn, B. Kippelen, J.-L. Brédas, S. R. Marder, *J. Mater. Chem.* **2008**, *18*, 3157.

[7] Y. Dong, J. W. Y. Lam, Z. Li, A. Qin, H. Tong, Y. Dong, X. Feng, B. Z. Tang, *J. Inorg. Organomet. Polym. Mater.* **2005**, *15*, 287 – 291.

[8] a) G. Yu, S. W. Yin, Y. Q. Liu, J. S. Chen, X. J. Xu, X. B. Sun, D. G. Ma, X. W. Zhan, Q. Peng, Z. G. Shuai, B. Z. Tang, D. B. Zhu, W. H. Fang, Y. Luo, *J. Am. Chem. Soc.* **2005**, *127*, 6335 – 6346; b) Y. N. Hong, J. W. Y. Lam, B. Z. Tang, *Chem. Commun.* **2009**, 4332 – 4353.

[9] a) Q. Y. Wu, Q. Peng, T. Zhang, Z. G. Shuai, *Sci. Sin. Chim.* **2013**, *43*, 1078 – 1089; b) T. Zhang, Y. Q. Jiang, Y. L. Niu, D. Wang, Q. Peng, Z. G. Shuai, *J. Phys. Chem. A* **2014**, *118*, 9094 – 9104.

[10] C. M. Deng, Y. L. Niu, Q. Peng, Z. G. Shuai, *Acta Phys. Chim. Sin.* **2010**, *26*, 1051 – 1058.

[11] A. Dreuw, M. Head-Gordon, *Chem. Rev.* **2005**, *105*, 4009 – 4037.

[12] a) H. Uoyama, K. Goushi, K. Shizu, H. Nomura, C. Adachi, *Nature* **2012**, *492*, 234 – 238; b) R. Ishimatsu, S. Matsunami, K. Shizu, C. Adachi, K. Nakano, T. Imato, *J. Phys. Chem. A* **2013**, *117*, 5607 – 5612.

[13] a) Q. Y. Wu, T. Zhang, Q. Peng, D. Wang, Z. G. Shuai, *Phys. Chem. Chem. Phys.* **2014**, *16*, 5545 – 5552; b) Z. G. Shuai, Q. Peng, *Phys. Rep.* **2014**, *537*, 123 – 156; c) Q. Y. Wu, C. M. Deng, Q. Peng, Y. L. Niu, Z. G. Shuai, *J. Comput. Chem.* **2012**, *33*, 1862 – 1869; d) Q. Peng, Y. P. Yi, Z. G. Shuai, J. S. Shao, *J. Am. Chem. Soc.* **2007**, *129*, 9333 – 9339; e) Z. G. Shuai, D. Wang, Q. Peng, H. Geng, *Acc. Chem. Res.* **2014**, *47*, 3301 – 3309.

[14] a) Z. G. Shuai, W. Xu, Q. Peng, H. Geng, *Sci. China Chem.* **2013**, *56*, 1277 – 1284; b) Z. G. Shuai, W. J. Liu, W. Z. Liang, Q. Shi, H. Chen, *Sci. China Chem.* **2013**, *56*, 1258 – 1262.

[15] X. Gao, Q. Peng, Y. L. Niu, D. Wang, Z. G. Shuai, *Phys. Chem. Chem. Phys.* **2012**, *14*, 14207 – 14216.

[16] R. Ahlrichs, M. Bär, M. Häser, H. Horn, C. Kölmel, *Chem. Phys. Lett.* **1989**, *162*, 165 – 169.

[17] a) J. Aaqvist, A. Warshel, *Chem. Rev.* **1993**, *93*, 2523 – 2544; b) H. Lin, D. G. Truhlar, *Theor. Chem. Acc.* **2007**, *117*, 185 – 199.

[18] J. M. Wang, R. M. Wolf, J. W. Caldwell, P. A. Kollman, D. A. Case, *J. Comput. Chem.* **2004**, *25*, 1157 – 1174.

[19] P. Sherwood, A. H. de Vries, M. F. Guest, G. Schreckenbach, C. R. A. Catlow, S. A. French, A. A. Sokol, S. T. Bromley, W. Thiel, A. J. Turner, S. Billeter, F. Terstegen, S. Thiel, J. Kendrick, S. C. Rogers, J. Casci, M. Watson, F. King, E. Karlsen, M. Sjøvoll, A. Fahmi, A. Schäfer, C. Lennartz, *THEOCHEM* **2003**, *632*, 1 – 28.

[20] W. Smith, T. R. Forester, *J. Mol. Graphics* **1996**, *14*, 136 – 141.

[21] S. H. Lin, C. H. Chang, K. K. Liang, R. Chang, Y. J. Shiu, J. M. Zhang, T.-S. Yang, M. Hayashi, F. C. Hsu, *Adv. Chem. Phys.* **2002**, *121*, 1 – 88.

[22] a) Y. L. Niu, Q. Peng, Z. G. Shuai, *Sci. China Ser. B* **2008**, *51*, 1153 – 1158; b) Q. Peng, Y. P. Yi, Z. G. Shuai, J. S. Shao, *J. Chem. Phys.* **2007**, *126*, 114302.

[23] Y. Y. Niu, Q. Peng, Q. Shi, X. Gao, Z. G. Shuai, *J. Chem. Theory Comput.* **2013**, *9*, 1132 – 1143.

[24] Q. Peng, Y. L. Niu, C. M. Deng, X. Gao, Z. G. Shuai, *J. Phys. Chem. A* **2010**, *114*, 7817 – 7831.

[25] J. R. Reimers, *J. Chem. Phys.* **2001**, *115*, 9103.

[26] R. Send, F. Furche, *J. Chem. Phys.* **2010**, *132*, 044107.

[27] Z. D. Li, B. Suo, Y. Zhang, Y. L. Xiao, W. J. Liu, *Mol. Phys.* **2013**, *111*, 3741 – 3755.

[28] Z. D. Li, Y. L. Xiao, W. J. Liu, *J. Chem. Phys.* **2012**, *137*, 154114.

[29] W. J. Liu, G. Hong, D. Dai, L. M. Li, M. Dolg, *Theor. Chem. Acc.* **1997**, *96*, 75 – 83.

[30] Z. G. Shuai, Q. Peng, Y. L. Niu, H. Geng, MOMAP, a free and open-source molecular materials property prediction package, Revision 0.2.004; available online: http://www.shuaigroup.net/, Beijing, China, **2014**.

Manuscript received: March 30, 2015
Accepted Article published: June 17, 2015
Final Article published: July 3, 2015